Journal of *Marine Science and Engineering*

MDPI

Article

Experimental Research on the Propagation Mode of 3D Hollow Cracks and Material Strength Characteristics Under Hydro-Mechanical Coupling

Bangxiang Li, Guanhua Wang, Dongyang Xu and Hongbo Zhao *

School of Civil Engineering and Geomatics, Shandong University of Technology, Zibo 255000, China; libangxiang@126.com (B.L.); aa041116@icloud.com (G.W.)
* Correspondence: bxhbzhao@hotmail.com or hbzhao@sdut.edu.cn

Abstract: The fracture evolution and the strength characteristics of a jointed rock mass under hydro-mechanical coupling are key issues that affect the safety and stability of underground engineering. In this study, a kind of transparent rock-like resin was adopted to investigate the crack initiation and propagation modes of the 3D flaw under hydro-mechanical coupling. The influences of the water pressure and the flaw dip angle on the fracture modes of the 3D flaw and the strength properties of the specimen were analyzed. The experiment results indicated that under the initiation and propagation modes, the 3D flaw presented two types of modes: the low-water-pressure type and the high-water-pressure type. The increase in the water pressure had a significant promoting effect on the crack initiation and propagation, which changed the overall failure mode of the specimen. With the increase in the flaw dip angle, the critical growth length of the wing crack decreased and the initiation moment of the fin-like crack showed a hysteretic tendency. The influences of the water pressure on the crack initiation stress and failure strength had thresholds. When lower than the threshold, the crack initiation stress increased slightly and the failure strength decreased gradually with the increase in the water pressure. Once the threshold was exceeded, both the crack initiation stress and the failure strength decreased significantly with the increase in the water pressure. With the increase in the flaw dip angle, both the crack initiation stress and the failure strength showed a first decreasing and then increasing tendency. The lowest crack initiation stress and the failure strength were found for the specimen containing the 45° flaw, while the highest were found for the specimen containing the 75° flaw. This study helps to deepen the understanding of the fracture mechanism of the engineering rock mass under hydro-mechanical coupling and has certain theoretical and applied value in engineering design and construction safety.

Keywords: 3D crack; crack initiation stress; failure strength; hydro-mechanical coupling; initiation and propagation mode

check for updates

Academic Editor: José António Correia

Received: 28 December 2024
Revised: 25 January 2025
Accepted: 27 January 2025
Published: 30 January 2025

Citation: Li, B.; Wang, G.; Xu, D.; Zhao, H. Experimental Research on the Propagation Mode of 3D Hollow Cracks and Material Strength Characteristics Under Hydro-Mechanical Coupling. *J. Mar. Sci. Eng.* **2025**, *13*, 259. https://doi.org/10.3390/jmse13020259

Copyright: © 2025 by the authors. Licensee MDPI, Basel, Switzerland. This article is an open access article distributed under the terms and conditions of the Creative Commons Attribution (CC BY) license (https://creativecommons.org/licenses/by/4.0/).

1. Introduction

In recent years, significant progress has been made in the construction of submarine tunnels around the world [1,2], such as the Hong Kong-Zhuhai-Macao Bridge Undersea Tunnel [3–5], Seikan Tunnel [6], and Rogfast Tunnel [7]. These projects faced extremely complex geological environments. The rock mass in submarine tunnels was not only subject to the geostress but also to the strong action of high seepage pressure. For example, the Qingdao Second Submarine Tunnel under construction [8], which is expected to be the world's longest undersea highway tunnel, faces a complex engineering environment of

1 MPa water pressure and the crossing of several fracture zones along the whole route. Under the blasting impact and excavation disturbance, the high-pressure water can easily enter the fracture zone, inducing the joints and fractures to propagate and coalesce under the coupling of the high geostress and high seepage pressure, leading to the instability and collapse of the rock mass, seriously threatening the structural safety and stability of the surrounding rock mass in subsea tunnels. Therefore, it is of great significance to study the failure mechanism of fractured rock masses under hydro-mechanical coupling for guiding the design, construction, and operation and maintenance of subsea tunnels.

For crack propagation under hydro-mechanical coupling, most of the previous scholars simplified the flaw into a 2-D penetration model and carried out a large number of fundamental studies by using theoretical analyses and numerical simulations [9–15]. The influences of the water pressure on the crack initiation and propagation of the 2-D flaw were investigated, and the crack initiation criterion under hydro-mechanical coupling was proposed. Moreover, the fracture mechanism of the fractured rock mass under hydro-mechanical coupling was analyzed. However, the CT tomography shows that the pre-existing discontinuities in engineering rocks are usually in a 3D form rather than a 2D form [16], and investigating the crack propagation mode from a 3D pre-existing flaw under hydro-mechanical coupling is more suitable for engineering practice [17].

The initiation and propagation of 3D discontinuities under the hydro-mechanical coupling commonly found in engineering surrounding rock is complicated. Up to now, scholars have carried out a large number of studies on the hydraulic fracture of rock masses [18–31] to investigate the propagation shapes of the fracture under different stress environments, and the law of the influence of natural cracks on hydraulic crack propagation were analyzed. Mei et al. [32,33] conducted hydro-mechanical coupling fracture tests on the mortar specimens containing single internal 3-D cracks, and the influences of the water pressure on the failure modes were analyzed. Du et al. [34] performed hydro-mechanical coupling tests on sandstones with two fissures, and the behaviors in the strength, deformation, permeability, and failure mode of sandstone were fully explored.

Given the opacity of rock and the rock-like material, such as mortar or the gypsum, the initiation and propagation process of the 3D crack cannot be observed. The influences of hydro-mechanical coupling on the development of a 3D crack are still unclear. Therefore, some scholars have turned to using transparent rock-like media to study the propagation of 3D cracks [35–37]. Dyskin et al. [38] used a transparent casting resin to fabricate samples with single internal 3D cracks and performed a uniaxial compressive test. The influence of the shape and locations of the initial 3D cracks on their growth were investigated. Moreover, the intrinsic limits on 3D crack growth were found, and the maximum possible size of wing cracks was about a comparable size of the initial crack. Wang et al. [39–41] used the same resin material to conduct a biaxial compressive test and found that the wing crack grew extensively. Zhou et al. [42] investigated the crack initiation, growth, wrapping, and coalescence of two 3D pre-existing cross-embedded flaws using a PMMA specimen, and four modes of crack initiation and five modes of crack coalescence were observed.

However, the above studies mainly focused on the initiation and propagation of the 3D crack in a pure stress environment and did not consider the influences of the water pressure on the development of the 3D crack. Recently, some exploratory studies have been performed using transparent rock-like material to investigate the propagation mode of 3D cracks under hydro-mechanical coupling. Cao et al. [36] investigated the crack initiation stress and failure strength of specimens containing a 3D crack group under 2 MPa water pressure, and the influences of the flaw dip angle and spacing of crack group were analyzed based on the propagation test of the 3D crack group under single water pressure conditions. However, the brittleness and the resin (the ratio of the tensile strength to the compressive

strength) used in Cao's tests was only 6.1, much lower than those of typical rocks (usually range from 10 to 20). Fu et al. [35,43] studied the crack initiation and propagation process of cracks under internal water pressure, described the growth mode of secondary cracks, and compared the similarities and differences of specimens under two water pressure conditions. However, Fu's study mainly focused on the propagation modes of the 3D crack and neglected the mechanical properties of the specimen.

To further clarify the crack initiation and propagation mechanism of 3D flaws under hydro-mechanical coupling and reveal the influences of the hydro-mechanical coupling fracture of the strength properties of the rock, this paper adopted transparent resin material to carry out hydro-mechanical coupling fracture tests. Based on the test results, the crack initiation and propagation modes of the 3D hollow flaw were summarized systematically, and the influences of the water pressure and the flaw dip angle on the crack initiation stress and failure strength of specimens were analyzed. This study helps to deepen the understanding of the evolutionary mechanism of the fracture of the engineering rock mass under hydro-mechanical coupling and has certain theoretical and applied value in engineering design and construction safety.

2. Specimen Preparation and Test Method

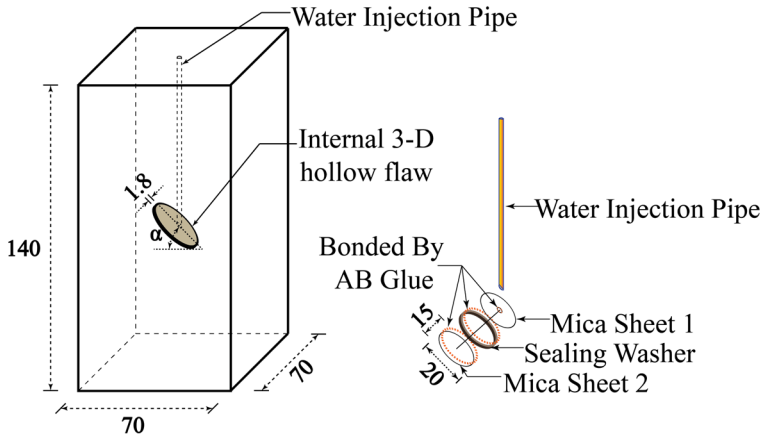
2.1. Test Material and Specimen Preparation

Given the non-transparent property of the rock, the propagation of the internal crack cannot be directly observed. Therefore, the transparent rock-like resin material developed in the literature [44,45] was adopted to prepare specimens. The ratio of the tensile strength to the compressive strength of the resin was 1/9.98 at a temperature of −45 °C, which is close to typical rocks, such as marble and sandstone [46]. The fracture toughness of the resin was about 0.55 MPa·m$^{1/2}$ at a temperature of −40 °C, which is also close to that of sandstone. Moreover, this material had excellent transparency. The comparison of mechanical parameters between the resin material and typical rocks is shown in Table 1. One thing to point out is that the resin is a polymer without micro pores, which can be widely found in rocks. Therefore, the effects of the seepage flow on the fracture behavior were not considered in this study.

Table 1. Comparison of mechanical parameters between resin and typical rocks (units: MPa).

Mechanical Parameter	Improved Resin	Sandstone	Granodiorite	Marble
Uniaxial compressive strength	121.3	105.3	148.3	101.6
Tensile Strength	12.2	9.5	16.0	10.1
Tensile Compressive Strength Ratio	1/9.98	1/11.08	1/9.27	1/10.06

The size of the specimen was 70 × 70 × 140 mm. To study the crack initiation and propagation modes of the 3D flaw under hydro-mechanical coupling, a 3D hollow elliptical flaw was preset at the center of the specimen, of which the size was 20 × 15 mm (long axis × short axis) and the thickness was 1.8 mm. The hollow flaw was constituted of two mica sheets, a washer, and a water injection pipe, which were glued together to form an inside cavity. The water pressure can be applied to the inside of the flaw through the water injection pipe during the test [35]. For the no-water pressure condition, no water injection pipe was set, and the hollow flaw was sealed. The dimensions and the structures of the specimen and the hollow flaw are shown in Figure 1.



(**a**) Specimen shape and size (**b**) Hollow flaw structure and size

Figure 1. The sizes and structures of the specimen and 3-D hollow flaw (units: mm).

To study the influences of the flaw dip angle and the water pressure on the initiation and propagation modes of the 3-D flaw and the strength characteristics of the specimens, the flaw dip angle α was set as 30°, 45°, 60, and 75°, and four kinds of water pressures were set: 0 MPa (no water pressure), 0.5 MPa, 2 MPa, 4 MPa. To reduce the dispersion of the test results, 3 specimens (48 specimens in total) were prepared for the same condition, and the average values of the test data were taken for the analysis.

2.2. Test Method

In the test, a WAW-1000C hydro-mechanical coupling servo testing machine was used to apply the axial uniaxial load, and a servo-controlled high-pressure water injection device was used to provide stable water pressure to the flaw. At the beginning of the test, an axial load of 1 kN was applied to the specimen so that the water injection platen closely adhered to the upper surface of the specimen. Then, the water pressure was applied to the target value and kept constant. Finally, the axial compression load was applied until the failure of the specimen.

To ensure that the specimen maintained a high degree of brittleness, the specimen was frozen to an ultra-low-temperature of −45 °C before the test and then put into a self-designed low-temperature environment box for the test. A large amount of dry ice was placed in the environment box to keep the temperature of the specimen at about −40 °C, which effectively avoided the influence of the temperature rise on the brittleness of the specimen. During the test, an infrared thermometer was used to monitor the temperature of the specimen. When the rising temperature was found to exceed 2 °C, more dry ice was supplemented to lower the temperature.

For the specimen in the water injection condition, it was necessary to fill the hollow flaw with antifreezing liquid, which was a mixture containing water and alcohol, before freezing. The freezing point of the antifreezing liquid was about −52 °C, which prevented it from freezing at a low temperature and ensured the water pressure to effectively transmit to the interior of the hollow flaw. To observe the propagation and evolutionary process of the crack more clearly, a kind of red dye was added to the antifreezing liquid to highlight the shape of the crack.

3. Initiation and Propagation Modes of 3-D Flaw Under Hydro-Mechanical Coupling

Rock fracture tests under hydro-mechanical coupling were carried out to summarize the basic features of the crack initiation and propagation of the 3D flaw. With variations in

the water pressure and the flaw dip angle, the influences of the water pressure and flaw dip angle on crack initiation and propagation modes were analyzed.

3.1. Basic Characteristics of 3D Crack Initiation and Propagation

In the hydro-mechanical coupling rock fracture test, different types of new cracks initiated from the 3D flaw duo to the increasing loading [47]. To facilitate the analysis, the new cracks were named according to their initiation locations and propagation patterns, and the basic characteristics of each type of new crack were summarized, as shown in Figure 2.

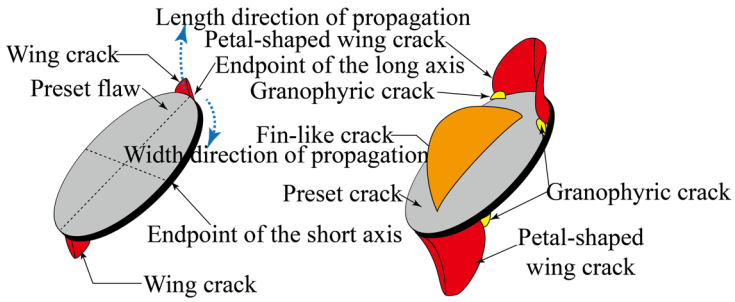


Figure 2. Types and propagation modes of newly generated cracks.

The wing cracks initiated at the tips of the preset 3D flaw (the endpoint of the long axis), and the initiation direction was approximately perpendicular to the preset flaw surface. With an increase in the load, in the length direction, the wing crack gradually turned to the direction of the maximum principal stress; in the width direction, the wing crack propagated along the edge of the preset flaw, forming a petal-shaped wing crack. When the propagation of the petal-shaped wing crack was close to reaching the end point of the short-axis, the wrapped wing crack was formed.

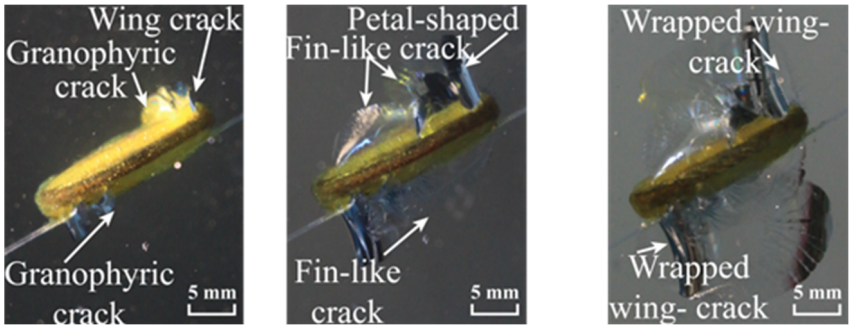
The granophyric crack initiated at the edges of preset crack, its location was close to the propagation front of the wing crack along the width direction, and its strike was at a small angle with the edge of the preset crack. The granophyric crack induced the wing crack to propagate further along the width direction, which led to it being merged with the wing crack.

The fin-like cracks initiated on the upper or lower surface of the preset crack, and their propagation direction was approximately perpendicular to the upper and lower surfaces of the preset cracks and generally along the long axis of the preset crack. The initiation and propagation of the fin-like crack was almost instantaneously completed, and the presence of the fin-like cracks reduced the propagation velocity of the wing cracks to a certain extent.

3.2. Three-Dimensional Crack Initiation and Propagation Modes Under Hydro-Mechanical Coupling

3.2.1. Crack Initiation and Propagation Modes Under No-Water Conditions

Firstly, the fracture test under no-water conditions was carried out. Under the axial loads, the initiation and propagation modes of the 3D hollow flaw had similarities with the closed flaw, which was described in the literature [44] (Figure 3). The wing cracks initiated at the tips of the flaw. With an increase in the load, the wing crack gradually grew into a petal wing crack. During this period, the granophyric crack kept initiating and was merged with the wing crack, forming wrapped wing cracks.



(**a**) Initiation stage (**b**) Stable propagation stage (**c**) Critical propagation stage

Figure 3. Initiation and propagation modes of 3D crack without hydro-pressure.

Meanwhile, the initiation and propagation modes of the hollow flaw were significantly different from those of the closed cracks. During the propagation of the wing crack, fin-like cracks initiated on the upper and lower surfaces of the hollow flaw, which was not observed in the closed crack condition. In addition, the wing crack initiated from a closed flaw propagated continuously, which eventually led to the failure of the specimen [44]. While the wing crack that initiated from a hollow flaw stopped propagating after reaching the critical length, this could not directly lead to the failure of the specimen. This phenomenon was consistent with the self-limiting effect of the propagation of the wing cracks proposed by Dyskin [38,48]. Since it was impossible to inject high-pressure water into the closed flaw, the comparison between the hollow flaw and the closed cracks was only confined to the no-water condition.

The analysis showed that the initiation of the fin-like crack was related to the cavity in the hollow flaw. With an increase in the axial load, the upper and lower surfaces of the crack gradually bent and deformed into the cavity, resulting in the concentration of tensile stress on the surfaces. When the tensile stress exceeded the tensile strength of the material, a fin-like crack initiated on the crack surface. The initiation of the fin-like crack reduced the stress concentration around the crack and slowed down the propagation of the wing crack. Meanwhile, compared to the size of the flaw, the size of the specimen was relatively large, and the material around the flaw had a significant self-limiting effect on the propagation of the wing crack, which made it difficult to continuously propagate after reaching the critical length.

3.2.2. Crack Initiation and Propagation Modes Under Hydro-Mechanical Coupling

Under hydro-mechanical coupling, the crack initiation and propagation modes of the 3D flaw were significantly different from those under the no-water conditions. The degree of the difference was related to the magnitude of the water pressure. In this research, the water pressure was divided into two types: low water pressure (0~2 MPa) and high water pressure (2~4 MPa).

The crack initiation and propagation modes under the low water pressure are shown in Figure 4 (taking 0.5 MPa water pressure as an example). When the axial load reached about 35% of the failure strength, multiple small cracks first initiated at the tips of the flaw. With the increase in the load, the small cracks gradually merged into the wing crack, and the pressurized water invaded the wing cracks, driving them to propagate steadily and to form the petal wing cracks. During the steady propagation of the wing crack, the fin-like cracks appeared successively on the upper and lower surfaces of the flaw. When the axial load increased to about 80% of the failure strength, the wing crack propagated to the critical length, forming a wrapped wing crack and stopping propagating. When the axial load approached the failure strength, macroscopic crack surfaces were formed in other regions

of the specimen, coalescing with the wing cracks and the fin-like cracks, which led to the overall failure of the specimen.

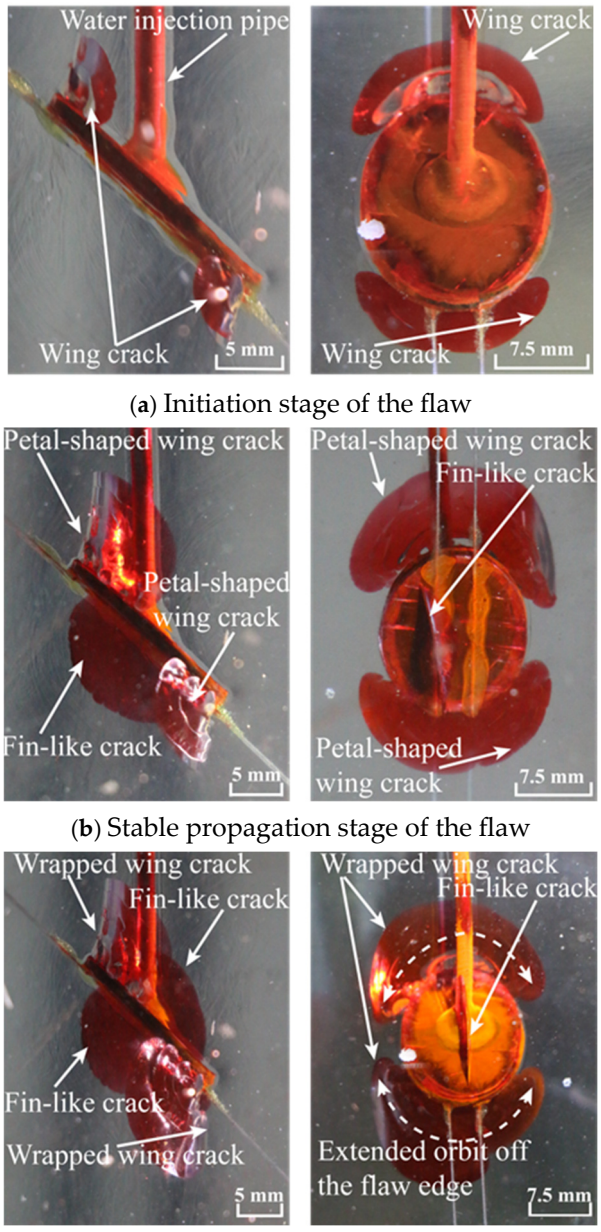
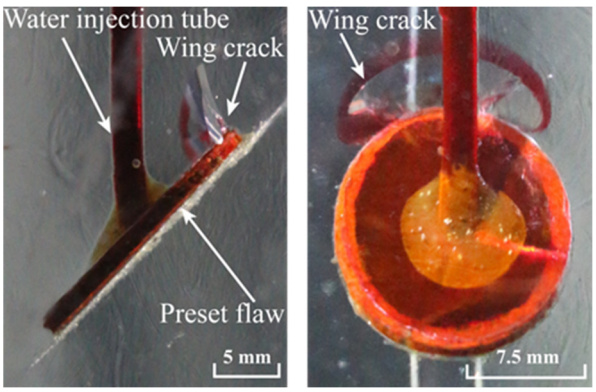
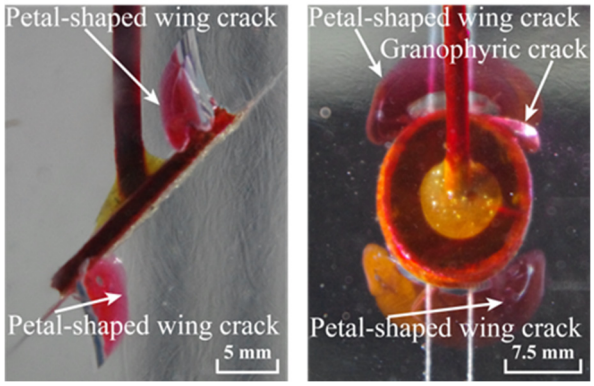


Figure 4. Initiation and propagation modes of 3D crack under low hydro-pressure conditions (e.g., hydro-pressure is 0.5 MPa).

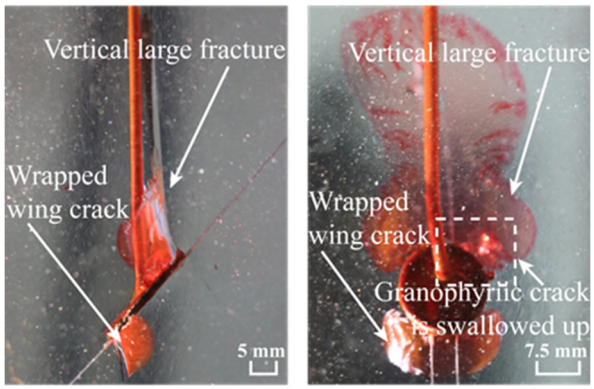
The crack initiation and propagation modes under high water pressure are shown in Figure 5 (taking 4 MPa water pressure as an example). In this condition, the load corresponding to the crack initiation was also about 35% of the failure strength. However, the failure strengths under high water pressure were much lower than those under low water pressure. The high water pressure and the axial load induced the wing cracks to initiate instantaneously and propagated rapidly into the petal wing cracks, which then propagated steadily to form the wrapped wing cracks. When the load reached about 85% of the failure strength, the wrapped wing crack stopped propagating temporarily. Then, the wrapped wing crack entered an unstable propagation state and grew rapidly to become a vertical large fracture, resulting in the failure of the specimen.



(**a**) Initiation stage of the flaw



(**b**) Stable propagation stage of the flaw



(**c**) Unstable stage of the flaw

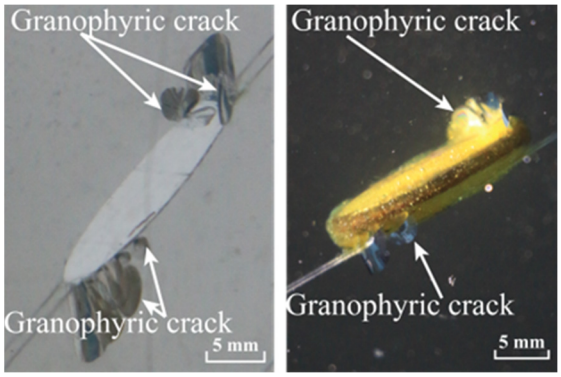
Figure 5. Initiation and propagation modes of 3D crack under high hydro-pressure conditions (e.g., hydro-pressure is 4 MPa).

In addition, the crack initiation and propagation process under high water pressure usually showed obvious asymmetry. The wing crack propagated rapidly after the initiation at one tip of the flaw, which relieved the stress concentration at another tip and delayed the initiation of the wing cracks. When the wing crack at one tip of the flaw reached the critical length, it first entered the unstable propagation state and formed a large vertical fracture surface.

3.3. Influences of Hydro-Mechanical Coupling on Crack Initiation and Propagation Modes

The influences of water pressure were mainly reflected in four aspects: the inhibitory effect on the initiation of the granophyric crack, the influence on the initiation timing of the fin-like cracks, the promoting effect on the crack initiation and propagation, and the influence on the final failure modes of the specimen.

Firstly, the presence of the water pressure inhibited the initiation of the granophyric crack. Under the no-water conditions, the granophyric crack initiated frequently at the stage of the wing crack initiation and propagation (Figure 6). The granophyric crack was difficult to observe under the presence of water pressure. It is inferred that the initiation of the granophyric crack was caused by the uneven distribution of the friction between the material and the flaw surface under the compressive shear stress, which caused a large stress concentration locally on the crack surface. When the stress exceeded the strength of the material, the granophyric crack initiated. Under the presence of water pressure, its lubrication and supporting effects on the flaw surface effectively relieved the uneven distribution of the friction, which made it difficult to produce granophyric cracks. The initiation of the granophyric cracks changed the propagation trajectory of the wing crack. Under no-water conditions, the initiation of the granophyric crack induced the wing crack to consistently propagate along the edge of the flaw. Under the presence of the water pressure, the granophyric crack was difficult to initiate, and the leading edges of the wing crack were somewhat detached from the flaw edges along the width direction; see Figure 4c.



(**a**) 3-D closed crack (**b**) 3-D opened crack

Figure 6. Initiation of granophyric cracks without hydro-pressure.

Secondly, the increase in water pressure delayed the initiation timing of the fin-like crack. Under the condition of no water or low water pressure, the fin-like cracks initiated rapidly on the upper and lower surfaces of the flaw. However, with the increase in the water pressure, the initiation timing was delayed. When the water pressure increased to 4 MPa, the fin-like cracks basically no longer initiated (Figure 5). It was analyzed that the water pressure in the crack partially offset the load borne by the surface of the hollow flaw and reduced the deflection deformation and tensile stress concentration on the upper and lower surfaces, which increased the axial load required for the initiation of the fin-like cracks.

Furthermore, the water pressure had an obvious promoting effect on the crack initiation and propagation. Under the conditions of no water and low water pressure, the formation of the wing crack was relatively slow. The process of wing crack initiation and propagation gradually accelerated with an increase in water pressure. When the water pressure increased to 4 MPa, the propagation of the wing crack was almost instantly completed. In addition, the increase in water pressure enhanced the propagation degree of the wing cracks, so that its critical propagation length increased continuously, as shown in Figure 7. Taking the 30° dip angle flaw as an example (Figure 8). When the water pressure increased from 0 MPa to 2 MPa, the critical propagation length of the wing crack grew from 0.58a to 1.58a (a is the length of the long axis of the preset crack). When the water pressure rose to 4 MPa, the wing crack continued to propagate, resulting in specimen splitting and failure. At this time, the critical propagation length did not exist. Under the condition of no water

or low water pressure, the 'self-limiting' effect made the critical propagation length of the wing crack exist [47,48]. The increase in water pressure exacerbated the normal dilatation effect at the leading edge of the wing crack propagation, which promoted the occurrence of crack at the leading edge of the propagation and effectively overcame the 'self-limiting' effect [38], and increased the critical propagation length.

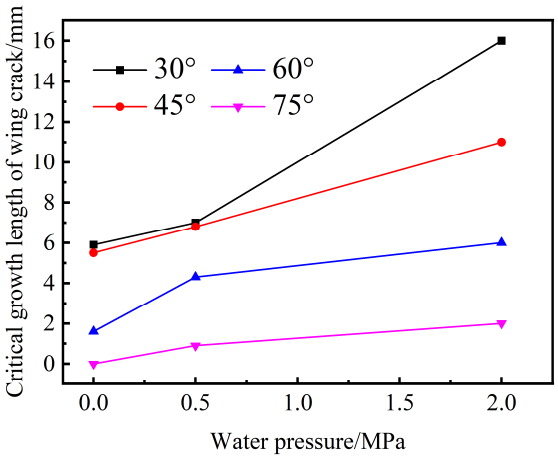
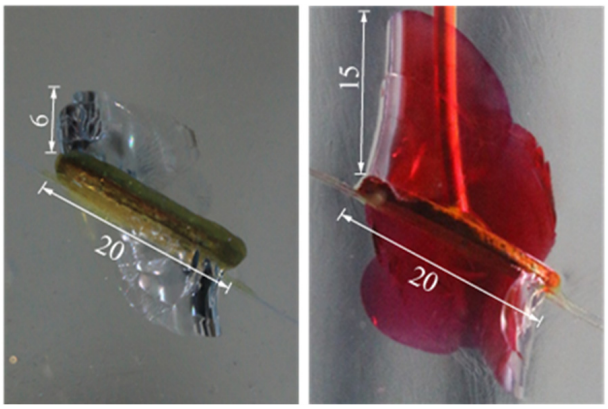


Figure 7. The influence of water pressure on the critical growth length of the wing crack.



(**a**) 0 MPa water pressure (**b**) 2 MPa water pressure

Figure 8. Critical growth lengths of wing cracks corresponding to different water pressures (e.g., flaw dip angle is 30°, unit: mm).

Finally, the water pressure had a significant effect on the final damage mode of the specimens. The damage modes of specimens corresponding to high and low water pressures are shown in Figure 9. Under the condition of no water or low water pressure, the wing crack stopped propagating after reaching the critical propagation length and when the external load increased to the ultimate bearing capacity of the material. A macroscopic rupture surface was generated inside the specimen, which lapped and passed through the wing and fin cracks, leading to the overall rupture of the specimen. Under high hydro-mechanical coupling, the wing cracks continued to propagate and penetrated into the surface of the specimen, forming a vertical large rupture surface, which led to the crack failure of the specimen.



(**a**) Low water pressure condition (**b**) High water pressure condition

Figure 9. Damage modes of specimen corresponding to different water pressures.

3.4. Influence of Dip Angle on the Modes of Crack Initiation and Propagation

The crack initiation and propagation mode was not only affected by the hydro-mechanical coupling but also related to the flaw dip angle. The experimental results showed that the influence of the flaw dip angle on the crack initiation and propagation mode was mainly manifested in two aspects: the critical propagation length of the wing crack and the timing of the emergence of the fin-like crack.

The influence of the flaw dip angle on the critical propagation length of wing cracks is shown in Figure 10. With the increase in the flaw dip angle, the critical propagation length of the wing crack decreased gradually. Taking the condition of 0.5 MPa water pressure as an example (Figure 11), when the flaw dip angle was 30°, the critical propagation length of the wing crack was about 0.70a (a is the length of the long semi-axis of the preset flaw), which was slightly larger than that of the 45° flaw, which was about 0.68a. When the flaw dip angle increased to 60°, the critical propagation length of the wing crack decreased to 0.42a. Moreover, the wing crack stopped propagating after the emergence of cracks at an angle of 75°. With an increase in the flaw dip angle, the crack initiation direction of the wing crack was gradually inclined horizontally. And the 'self-limiting' effect of the surrounding material on the propagation of the wing crack was strengthened under the action of the axial load, and the critical propagation length of the wing crack gradually decreased.

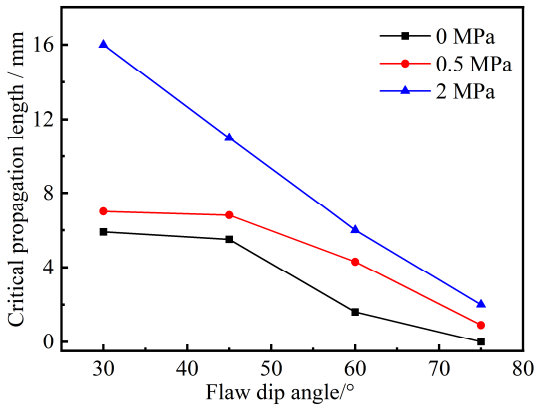
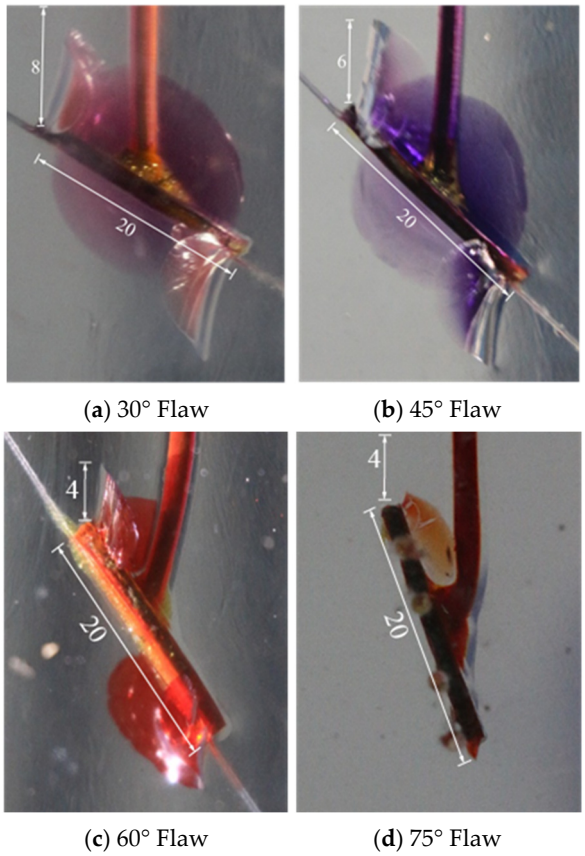


Figure 10. The influence of the flaw dip angle on the critical growth length of the wing crack.



(**a**) 30° Flaw (**b**) 45° Flaw

(**c**) 60° Flaw (**d**) 75° Flaw

Figure 11. Critical growth lengths of wing cracks corresponding to different flaw dip angles (e.g., hydro-pressure is 0.5 MPa, unit: mm).

On the other hand, the increase in the flaw dip angle led to a delayed trend in the initiation of the fin-like cracks. When the dip angle was 30°, the fin-like cracks initiated at the stable propagation stage of the wing crack. When the flaw dip angle was 45°, the fin-like cracks initiated before the wing cracks reached the critical propagation length. When the flaw dip angle increased to 60° or 75°, the emergence of fin-like cracks continued to be delayed or even no longer occurred. With an increase in the flaw dip angle, the axial load component in the normal direction of the crack surface decreased, and the deformation from the upper and lower surfaces of the hollow flaw to the interior decreased, which made it more difficult for the fin cracks to initiate, and the initiating timing was delayed.

4. Strength Properties of Specimen Containing 3D Hollow Flaw

To further reveal the strength properties of the rock containing a 3D flaw under hydro-mechanical coupling, the influences of the water pressure and the flaw dip angle on the crack initiation stress and failure strength were analyzed.

4.1. Influence of Water Pressure on Crack Initiation Stress and Failure Strength

4.1.1. Influence of Water Pressure on Crack Initiation Stress

The presence of water pressure largely changed the distribution of the stress field at the leading edge of the crack, which in turn had a significant influence on the crack initiation stress. The variation in the crack initiation stress with the change in the water pressure is shown in Figure 12 (the curve in the figure is plotted based on the average value of three specimens). For the 30°, 45°, and 60° flaws, the increase in water pressure in a small range led to a slight increase in the crack initiation stress. When the water pressure exceeded a certain threshold, the crack initiation stress decreased significantly. There were differences

in the threshold value of water pressure corresponding to the flaws with different dip angles. For the 75° flaw, the crack initiation phenomenon was not observed until the overall failure of the specimen initiated under the no-water condition. So there was no clear crack initiation stress.

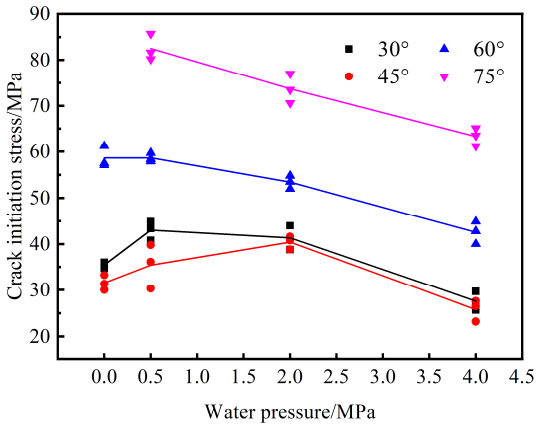


Figure 12. The influence of water pressure on crack initiation stress.

The analysis suggested that the emergence of the wing crack at the leading edge of the flaw under hydro-mechanical coupling was mainly caused by the combination of tension and shear stresses. As shown in Figure 13, the axial compressive load σ_1 could be decomposed into the normal stress σ_n and the shear stress τ on the flaw surface. The σ_n made the hollow flaw extruded and deformed, which led to the shear force f_s at the crack leading edge, while the shear stress τ prompted the upper and lowered surfaces of the crack to misalign with each other, which generated the tensile force t at the crack leading edge. The water pressure p_w produced an expansive effect on the top and bottom surfaces and the side of the flaw, which weakened the compressive effect of the axial load on the flaw surface and caused tensile stress σ_m at the tips of the flaw.

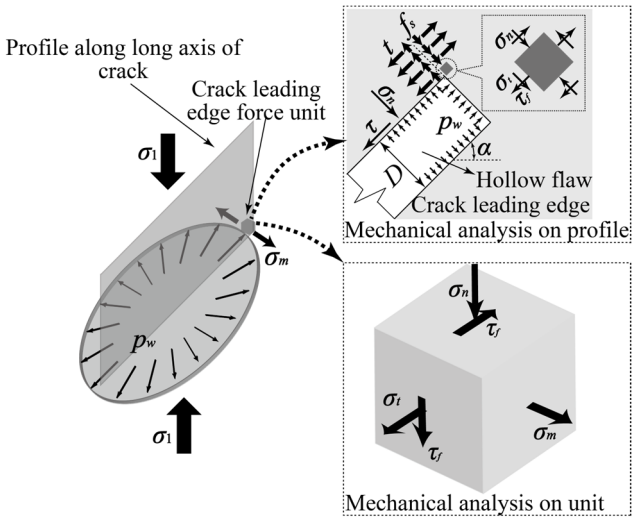


Figure 13. The mechanical analysis of the 3D hollow flaw under hydro-mechanical coupling.

Under the no-water condition, the crack leading edge unit was in a tension-shear state, which was easy to induce a tension-shear composite crack. Under the low-water-pressure condition, the pw partially offset the deflection of the flaw surface caused by the axial load, and the fs at the leading edge of the flaw was reduced, which inhibited the initiation of the shear crack and led to an increase in the crack initiation stress. After the water pressure

exceeded the threshold value, the tensile stress σ_m generated at the flaw tips increased significantly, which led to a significant decrease in the crack initiation stress. It could be inferred that with the increase in the water pressure, the contribution of the tension crack in the initiation of the wing crack was enhanced.

In addition, the test results showed that the hydro-mechanical coupling threshold tended to decrease with an increase in the crack dip angle. For 30° and 45° cracks, the thresholds were between 2 and 4 MPa, while the thresholds for 60° cracks are between 0.5 and 2 MPa.

4.1.2. Influence of Water Pressure on the Failure Strength of Specimens

The change in water pressure had a significant effect on the failure strength of the specimens. As shown in Figure 14, the failure strength decreased gradually with the increase in the water pressure. Under the conditions of low water pressure, the failure strength decreased relatively slowly with the increase in the water pressure, while under the conditions of high water pressure, the failure strength decreased rapidly.

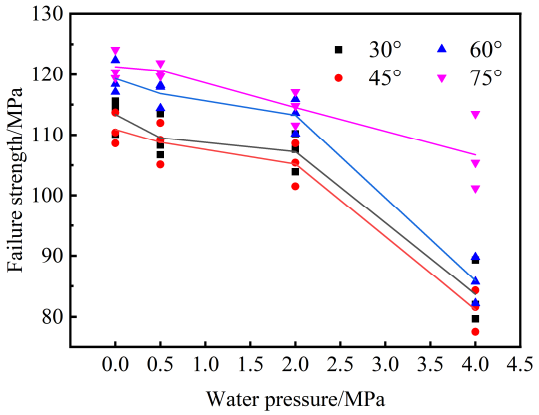


Figure 14. The influence of water pressure on the specimen failure strength.

In the range of the low water pressure, the critical propagation length of wing cracks increased to a limited extent with the increase in the water pressure, resulting in a slow decline in the failure strength of the specimen. In the range of high water pressure, the critical propagation length of the wing crack increased significantly with the water pressure, which was easy to induce the failure of the specimen and greatly reduced the failure strength of the specimen. The analysis showed that the influence of water pressure on the failure strength of the specimen also had a certain threshold value. When the threshold was exceeded, the high water pressure drove the wing crack to continuously propagate, resulting in a significant reduction in the failure strength.

4.2. Influence of Dip Angle on Crack Initiation Stress and Failure Strength

4.2.1. Influence of Dip Angle on Crack Initiation Stress

The change in the crack dip angle controlled the stress distribution around the flaw and influenced the crack initiation stress. The variation in the crack initiation stress with the dip angle is shown in Figure 15. It could be seen that the crack initiation stress under each water pressure condition decreased firstly and then increased with the increase in the flaw dip angle, among which the crack initiation stress of the 45° flaw was the lowest. Taking the 0.5 MPa water pressure as an example, when the flaw dip angle was 45°, the initiation stress was about 32.8% of the failure strength. The initiation stress of the 30° flaw was slightly higher than that of the 45° flaw, which was about 39.5% of the failure strength. The initiation stresses of the 60° and 75° flaws were significantly increased, which were

50.3% and 68.4% of the failure strength, respectively. In addition, the crack initiation of the 75° flaw was not observed under the condition of no-water pressure, so its initiation stress was not marked in the figure.

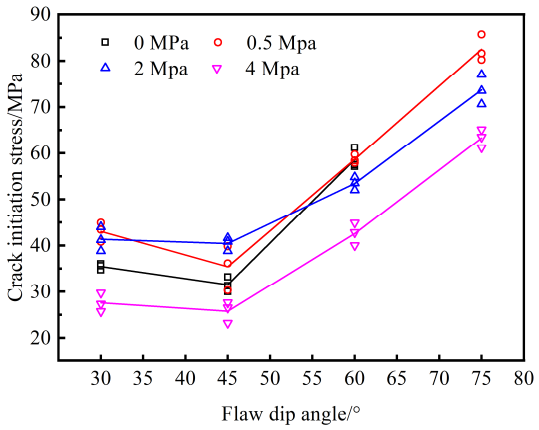


Figure 15. The influence of the flaw dip angle on the crack initiation stress.

It was analyzed that the specimen fracture angle was $\theta = \pi/4 + \varphi/2$ (where φ was the internal friction angle of the material) under the axial pressure condition [49]. When the dip angle was close to the fracture angle, the flaw tip was very easy to crack and the initiation stress was greatly reduced. In this study, the fracture angle of the transparent resin material was between 45° and 50°, leading to the lowest initiation stress at the 45° flaw.

The influence of the flaw dip angle on the crack initiation stress was closely related to the propagation degree of the wing crack. The test results showed that the critical propagation length of wing cracks was larger for the 30° and 45° flaw, because the crack initiation stress was lower and the wing crack can be fully propagated after initiation. The crack initiation stresses of 60° and 75° flaws were higher, and the specimens reached the failure strength soon after the initiation of the wing crack, so the critical propagation length of the wing crack was relatively small.

4.2.2. Influence of Flaw Dip Angle on the Failure Strength of Specimens

As shown in Figure 16, the influence of the flaw dip angle on the failure strength of the specimen was similar to that of the crack initiation stress. Under each water pressure condition, the failure strength of the specimens showed a tendency of decreasing first and then increasing with an increase in the flaw dip angle. Among them, the strength of the specimen with 45° flaw was the lowest, and the strength of the specimen with the 75° flaw was the highest.

Under the condition of no water or low water pressure, the differences in the failure strength with the variation in the flaw dip angle were small. That was because the failure modes of the specimens were overall failure. However, due to the fact that the initiation stress of the 45° flaw was the lowest, the weakening effect of the wing crack on the load-bearing capacity of the specimen of the greatest, which led to the lowest failure strength. Under high water pressure, the wing crack was driven to continuously propagate, resulting in the splitting failure of the specimens containing the 30°, 45°, and 60° flaws. Therefore, their failure strengths were relatively close to each other. However, the failure mode of the specimen containing the 75° flaw was still overall failure, and its failure strength was higher than those of other specimens.

The variation of the crack initiation stress and the failure strength of specimens with the change in the flaw dip angle were basically same, which indicated that the crack initiation was closely related to the final failure for the brittle rock materials containing 3D

cracks. In addition, in the range of the dip angle in this experiment, the variation in the crack initiation stress was larger than that of the failure strength. Although the lowest crack initiation stress and failure strength were found for the specimen containing the 45° flaw, the loading process from the crack initiation to the final failure of the specimen was long and the safety reserve was high. However, the initiation stress and failure strength of the specimen containing the 75° flaw was the highest, but the loading process from the crack initiation to the failure of the specimen was short, and the safety reserve was relatively low.

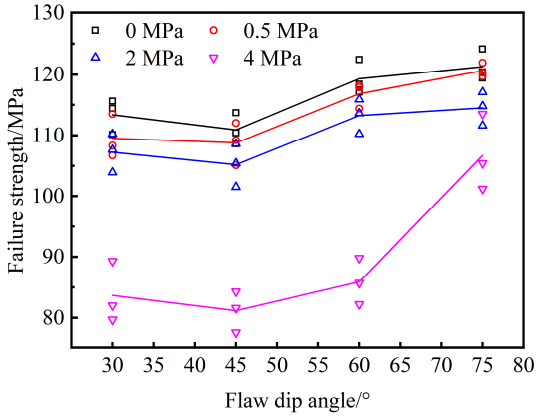


Figure 16. The influence of the flaw dip angle on the specimen failure strength.

5. Conclusions

Based on a transparent rock-like resin rock material with a brittleness of 1/9.98, a hydro-mechanical coupling fracture test was carried out in this paper. The basic modes of the crack initiation and propagation of the 3-D hollow flaw were summarized, and the crack initiation stress and the failure strength of the specimen were investigated. Moreover, the influences of the water pressure and the flaw dip angle on the development of the 3D crack and the mechanical properties of the specimen were analyzed. The main conclusions were as follows:

(1) There are three basic cracks initiating from the 3D preset flaw under hydro-mechanical coupling, which are wing cracks, granophyric cracks, and fin-like cracks. The characteristics of each basic crack were summarized.

(2) There are significant differences in the crack initiation and propagation modes between the no water condition and the hydro-mechanical coupling condition. The presence of water has an effective inhabitation on the initiation of the granophyric crack and the fin-like crack, which is related to the lubrication and supporting effects on the flaw surface of the high pressure water.

(3) The increase in the water pressure has a significant promoting effect on the development of the wing crack. The 3D crack initiation and propagation modes under hydro-mechanical coupling show two main types: the low water pressure type and the high water pressure type. Under low water pressure, the critical propagation length of the wing crack exists, and the failure mode of the specimen is overall failure. Under high water pressure, the wing crack continues to propagate, leading to the splitting failure of the specimen.

(4) There are thresholds for the influence of water pressure on the mechanical properties of the specimen. Before reaching the threshold, the crack initiation stress increases slightly with the increase in the water pressure. When the threshold is exceeded, the crack initiation stress and failure strength decreased rapidly.

(5) With the increase in the flaw dip angle, the crack initiation stress and the failure strength of the specimen show a trend of first decreasing and then increasing. Within

the range of the experiment, the lowest crack initiation stress and the failure strength of the specimens were found for the specimen containing the 45° flaw, while the highest crack initiation stress and the failure strength of the specimen were found for the specimen containing the 75° flaw.

Author Contributions: H.Z.: Conceptualization, Methodology, Writing—original draft, Supervision, Resources, Project administration. G.W.: Investigation, Validation, Writing—review and editing. D.X.: Validation, Writing—review and editing. B.L.: Visualization, Writing—review and editing. All authors have read and agreed to the published version of the manuscript.

Funding: The research reported in this paper was financially supported by the National Natural Science Foundation of China (Grant No. 52309137, 42377174), the China Postdoctoral Science Foundation (Grant No. 2024M751866), and the Natural Science Foundation of Shandong Province, China (Grant No. ZR2024QE218, ZR2022ME198).

Institutional Review Board Statement: Not applicable.

Informed Consent Statement: Not applicable.

Data Availability Statement: All data during this study are available from the corresponding author by request.

Conflicts of Interest: The authors declare no conflicts of interest.

References

1. Wang, T.; Xiang, Y.; Liu, L.; Xiong, W. Numerical Simulation of Construction Disturbances during Bidirectional Advancement of Undersea Large-Diameter Dual-Line Shield Tunneling. *J. Mar. Sci. Eng.* **2024**, *12*, 456. [CrossRef]
2. Guo, Y.; Li, X.; Fang, Y.; Jin, D.; Yang, Y.; Liu, H. Investigation into the pregelatinized starch additive alleviated the deterioration in rheological properties of slurries induced by high-temperature environment and seawater intrusion during submarine slurry shield tunneling. *Tunn. Undergr. Space Technol.* **2024**, *147*, 105693. [CrossRef]
3. Ma, P.; Wu, Z.; Zhang, Z.; Au, F.T.K. SAR-Transformer-based decomposition and geophysical interpretation of InSAR time-series deformations for the Hong Kong–Zhuhai–Macao Bridge. *Remote Sens. Environ.* **2024**, *302*, 113962. [CrossRef]
4. Ying, X.; Zheng, Z.; Ni, J.; Zhao, K. Numerical simulation study on the dynamic impact of typhoon "Mangkhut" storm surge on the sea area near the Hong Kong–Zhuhai–Macao bridge. *Phys. Chem. Earth Parts A/B/C* **2022**, *128*, 103269. [CrossRef]
5. Quanke, S.; Yongling, Z.; Yue, C.; Lei, F.; Yu, Y.; Zongxian, S.; de Wit, H.; Ying, L. Hong Kong Zhuhai Macao Bridge-Tunnel project immersed tunnel and artificial islands—From an Owners' perspective. *Tunn. Undergr. Space Technol.* **2022**, *121*, 104308. [CrossRef]
6. Ikuma, M. Maintenance of the undersea section of the Seikan Tunnel. *Tunn. Undergr. Space Technol.* **2005**, *20*, 143–149. [CrossRef]
7. Borg, A.; Bjelland, H.; Njå, O. Reflections on Bayesian Network models for road tunnel safety design: A case study from Norway. *Tunn. Undergr. Space Technol.* **2014**, *43*, 300–314. [CrossRef]
8. Shao, C.; Zhu, G.; Zhang, Q.; Duan, S.; Liu, R. Experimental study on sealing effect of cement–sodium silicate slurry in rock fracture with flowing seawater. *Tunn. Undergr. Space Technol.* **2025**, *155*, 106173. [CrossRef]
9. Huang, R.; Wang, X.; Chen, L. Hydro-splitting of analysis of underground water in deep-lying tunnels and its effect od water gushing out. *Chin. J. Rock Mech. Eng.* **2000**, *19*, 573–576.
10. Li, X.; He, X.; Chen, H. Crack initiation characteristics of opening-mode crack embedded in rock-like material under seepage pressure. *Chin. J. Rock Mech. Eng.* **2012**, *31*, 1317–1324.
11. Cappa, F.; Guglielmi, Y.; Fénart, P.; Merrien-Soukatchoff, V.; Thoraval, A. Hydromechanical interactions in a fractured carbonate reservoir inferred from hydraulic and mechanical measurements. *Int. J. Rock Mech. Min. Sci.* **2005**, *42*, 287–306. [CrossRef]
12. Li, Z.; Zhang, H.; Ren, Q.; Wang, Y. Analysis of hydraulic fracturing and calculation of critical internal water pressure of rock fracture. *Rock Soil Mech.* **2005**, *26*, 1216–1220. [CrossRef]
13. Pu, C.; Cao, P.; Zhang, C.; Fu, Z. Fracture failure mechanism of rock with closed crack and judging criterion of seepage pressure under biaxial compression. *Rock Soil Mech.* **2015**, *36*, 56–60 and 67. [CrossRef]
14. Zhao, Y.; Peng, Q.; Wan, W.; Wang, W.; Zhang, S. Seepage-fracture coupling mechanism of rock masses cracking propagationunder high hydraulic pressure and numerical verification. *Rock Soil Mech.* **2014**, *35*, 556–564. [CrossRef]
15. Zhao, Y.; Wang, W. Wing crack propagation model under high hydraulic pressure in compressive-shear stress state. *J. Coal Sci. Eng.* **2011**, *17*, 34–38. [CrossRef]
16. Bubeck, A.; Walker, R.J.; Healy, D.; Dobbs, M.; Holwell, D.A. Pore geometry as a control on rock strength. *Earth Planet. Sci. Lett.* **2017**, *457*, 38–48. [CrossRef]

17. Li, B.; Yu, S.; Zhu, W.; Cai, W.; Yang, L.; Xue, Y.; Li, Y. The Microscopic Mechanism of Crack Evolution in Brittle Material Containing 3-D Embedded Flaw. *Rock Mech. Rock Eng.* **2020**, *53*, 5239–5255. [CrossRef]
18. Heng, S.; Yang, C.; Zeng, Y.; Guo, Y.; Wang, L.; Hou, Z. Experimental study on hydraulic fracture geometry of shale. *Chin. J. Geotech. Eng.* **2014**, *36*, 1243–1251.
19. Pan, L.; Cheng, L.; Zhang, S.; Guo, T.; Liu, K. Mechanism of fracture propagation via numerical stimulation of reservoir volume fracture in shale reservoirs. *Rock Soil Mech.* **2015**, *36*, 205–211. [CrossRef]
20. Zhou, J.; Chen, M.; Jin, Y.; Zhang, G. Experimental study on propagation mechanism of hydraulic fracture in naturally fractured reservoir. *Acta Pet. Sin.* **2007**, *28*, 109–113.
21. Dam, D.B.v.; Papanastasiou, P.; de Pater, C.J. Impact of Rock Plasticity on Hydraulic Fracture Propagation and Closure. In Proceedings of the SPE Annual Technical Conference and Exhibition, Dallas, TX, USA, 1–4 October 2000; p. SPE–63172–MS.
22. Nordgren, R.P. Propagation of a Vertical Hydraulic Fracture. *Soc. Pet. Eng. J.* **1972**, *12*, 306–314. [CrossRef]
23. Gu, H.; Weng, X. Criterion For Fractures Crossing Frictional Interfaces At Non-orthogonal Angles. In Proceedings of the 44th U.S. Rock Mechanics Symposium and 5th U.S.-Canada Rock Mechanics Symposium, Salt Lake City, UT, USA, 27–30 June 2010; p. ARMA–10–198.
24. Gu, H.; Weng, X.; Lund, J.; Mack, M.; Ganguly, U.; Suarez-Rivera, R. Hydraulic Fracture Crossing Natural Fracture at Non-orthogonal Angles, A Criterion, Its Validation and Applications. In Proceedings of the SPE Hydraulic Fracturing Technology Conference, The Woodlands, TX, USA, 24–26 January 2011; p. SPE–139984-MS.
25. Renshaw, C.E.; Pollard, D.D. An experimentally verified criterion for propagation across unbounded frictional interfaces in brittle, linear elastic materials. *Int. J. Rock Mech. Min. Sci. Geomech. Abstr.* **1995**, *32*, 237–249. [CrossRef]
26. Bunger, A.; Kear, J.; Jeffrey, R.; Prioul, R.; Chuprakov, D. Investigation of hydraulic fracture growth through weak discontinuities with active ultrasound monitoring. *CIM J.* **2016**, *7*, 165–177. [CrossRef]
27. Fu, W.; Ames, B.C.; Bunger, A.P.; Savitski, A.A. Impact of Partially Cemented and Non-persistent Natural Fractures on Hydraulic Fracture Propagation. *Rock Mech. Rock Eng.* **2016**, *49*, 4519–4526. [CrossRef]
28. Yang, Y.; Yang, Y.; Ma, S.; Ju, Y.; Guo, Y.; Yu, Y. Crack propagation induced by hydraulic fracturing in low permeability rocks using CT technology. *J. Min. Saf. Eng.* **2013**, *30*, 739–743.
29. Li, S.; Zhao, H.; Cheng, T.; Wang, J.; Gai, J.; Zou, L.; He, T. The Analysis of Hydraulic Fracture Morphology and Connectivity under the Effect of Well Interference and Natural Fracture in Shale Reservoirs. *Processes* **2023**, *11*, 2627. [CrossRef]
30. Zheng, H.; Li, F.; Wang, D. Numerical Investigation of Complex Hydraulic Fracture Propagation in Shale Formation. *Processes* **2024**, *12*, 2630. [CrossRef]
31. Li, S.; Zhao, H.; Wang, J.; Xie, X.; Qin, L.; Zou, L.; Liu, Y. A Dynamic Propagation Numerical Model of Hydraulic Fracture Interactions with Pre-Existing Complex Natural Fractures. *Processes* **2024**, *12*, 899. [CrossRef]
32. Mei, J.; Yang, L.; Sheng, X.; Song, G.; Yang, W.; Zhang, B. Time-Dependent Propagation of 3-D Cracks in Rocks Under Hydromechanical Coupling. *Rock Mech. Rock Eng.* **2020**, *53*, 1923–1934. [CrossRef]
33. Yang, L.; Mei, J.; Sheng, X.; Yang, W.; Li, J. Cracking and Creep Behavior of Rocks Considering Propagation and Interaction of Adjacent Cracks Under Hydro-Mechanical Coupling. *Rock Mech. Rock Eng.* **2021**, *54*, 4099–4110. [CrossRef]
34. Du, Y.; Li, T.; Li, W.; Ren, Y.; Wang, G.; He, P. Experimental Study of Mechanical and Permeability Behaviors During the Failure of Sandstone Containing Two Preexisting Fissures Under Triaxial Compression. *Rock Mech. Rock Eng.* **2020**, *53*, 3673–3697. [CrossRef]
35. Fu, J.; Zhu, W.; Zhang, X.; Shi, L.; Xie, F. Fracturing experiment and numerical simulation study on new material containing a hollow internal crack under internal water pressure. *Adv. Eng. Sci.* **2017**, *49*, 78–85. [CrossRef]
36. Cao, J.; Zhu, Z.; Tian, Y.; Zhao, C.; Dong, X. The experimental study of propagation progress of 3d crack-SETS under hydraulic pressure. *Sci. Technol. Eng.* **2017**, *17*, 92–98.
37. Wan, B.; Liu, Y.; Zhang, B.; Luo, S.; Wei, L.; Li, L.; He, J. Investigation of the Vertical Propagation Pattern of the 3D Hydraulic Fracture under the Influence of Interlayer Heterogeneity. *Processes* **2022**, *10*, 2449. [CrossRef]
38. Dyskin, A.V.; Sahouryeh, E.; Jewell, R.J.; Joer, H.; Ustinov, K.B. Influence of shape and locations of initial 3-D cracks on their growth in uniaxial compression. *Eng. Fract. Mech.* **2003**, *70*, 2115–2136. [CrossRef]
39. Wang, H.; Dyskin, A.; Pasternak, E.; Dight, P. 3D Crack Growth in Biaxial Compression: Influence of Shape and Inclination of Initial Cracks. *Rock Mech. Rock Eng.* **2020**, *53*, 3161–3183. [CrossRef]
40. Wang, H.; Dyskin, A.; Pasternak, E. Comparative analysis of mechanisms of 3-D brittle crack growth in compression. *Eng. Fract. Mech.* **2019**, *220*, 106656. [CrossRef]
41. Wang, H.; Dyskin, A.; Pasternak, E.; Dight, P.; Sarmadivaleh, M. Experimental and Numerical Study into 3D Crack Growth from a Spherical Pore in Biaxial Compression. *Rock Mech. Rock Eng.* **2020**, *53*, 77–102. [CrossRef]
42. Zhou, X.-P.; Zhang, J.-Z.; Wong, L.N.Y. Experimental Study on the Growth, Coalescence and Wrapping Behaviors of 3D Cross-Embedded Flaws Under Uniaxial Compression. *Rock Mech. Rock Eng.* **2018**, *51*, 1379–1400. [CrossRef]
43. Fu, J.; Labuz, J.F.; Guo, M.; Cheng, H.; Hou, R. Experimental and numerical investigations on hydraulic fracture growth using rock-like resin material containing an injecting inner pre-crack. *J. Pet. Sci. Eng.* **2022**, *213*, 110424. [CrossRef]

44. Fu, J.; Zhu, W.; Luo, X.; Li, y.; Zhou, H.; Zhang, D. Study on failure process of fractured rock by using a new material containing three-dimensional internal fracture surfaces. *J. Cent. South Univ. Sci. Tech-Nology* **2014**, *45*, 3257–3263.
45. Fu, J.; Zhu, W.; Xie, F.; Xue, W.; Zhang, D.; Li, Y. Experi-mental studies and elastic-brittle simulation of propagation and coalescence process of two three-dimensional flaws in rocks. *Rock Soil Mech.* **2013**, *34*, 2489–2495. [CrossRef]
46. Perras, M.A.; Diederichs, M.S. A Review of the Tensile Strength of Rock: Concepts and Testing. *Geotech. Geol. Eng.* **2014**, *32*, 525–546. [CrossRef]
47. Wong, R.H.C.; Law, C.M.; Chau, K.T.; Zhu, W.-S. Crack propagation from 3-D surface fractures in pmma and marble specimens under uniaxial compression. *Int. J. Rock Mech. Min. Sci.* **2004**, *41*, 360. [CrossRef]
48. Dyskin, A.V.; Jewell, R.J.; Joer, H.; Sahouryeh, E.; Ustinov, K.B. Experiments on 3-D crack growth in uniaxial compression. *Int. J. Fract.* **1994**, *65*, R77–R83. [CrossRef]
49. Cai, M.; He, M.; Liu, D. *, (Eds.) Rock Mechanics and Engineering*; Science Press: Beijing, China, 2002.

Disclaimer/Publisher's Note: The statements, opinions and data contained in all publications are solely those of the individual author(s) and contributor(s) and not of MDPI and/or the editor(s). MDPI and/or the editor(s) disclaim responsibility for any injury to people or property resulting from any ideas, methods, instructions or products referred to in the content.